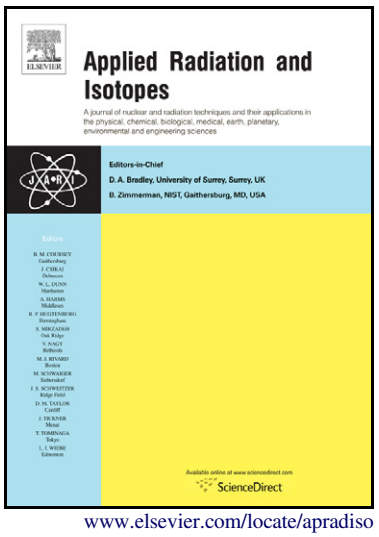

www.elsevier.com/locate/apradiso

Water equivalent properties of materials commonly used in proton dosimetry

Pablo de Vera, Isabel Abril, Rafael Garcia-Molina

PII: S0969-8043(13)00024-9
DOI: http://dx.doi.org/10.1016/j.apradiso.2013.01.023
Reference: ARI6086

To appear in: *Applied Radiation and Isotopes*

Cite this article as: Pablo de Vera, Isabel Abril and Rafael Garcia-Molina, Water equivalent properties of materials commonly used in proton dosimetry, *Applied Radiation and Isotopes,* http://dx.doi.org/10.1016/j.apradiso.2013.01.023

Water equivalent properties of materials commonly used in proton dosimetry

Pablo de Vera[1], Isabel Abril[1,*], Rafael Garcia-Molina[2]

[1]Departament de Física Aplicada, Universitat d'Alacant, E-03080 Alacant, Spain

[2]Departamento de Física – CIOyN, Universidad de Murcia, E-30100 Murcia, Spain

Abstract

The depth dose distribution of proton beams in materials currently used in dosimetry measurements, such as liquid water, PMMA or graphite are calculated with the SEICS (Simulation of Energetic Ions and Clusters through Solids) code, where all the relevant effects in the evaluation of the energy deposited by the beam in the target are included, such as electronic energy-loss (including energy-loss straggling), multiple elastic scattering, electronic charge-exchange processes, and nuclear fragmentation interactions. Water equivalent properties are obtained for different proton beam energies and several targets of interest in dosimetry.

Keywords: hadronteraphy, proton beam, Bragg peak, dosimetry, liquid water, water equivalent properties

* Corresponding author: Fax: +34 965909726. E-mail address: ias@ua.es (I. Abril).

1.- Introduction

Radiation oncology is one of the most recent applications of ion beams due to their well defined range and small angular scattering, as compared with conventional photon or electron beam radiotherapy. Heavy charged particles deposit most of their energy within a narrow depth near the end of their trajectories, with a pronounced dose peak, which is called the Bragg peak. An additional advantage is that they present an increased radiobiological effectiveness in the Bragg peak as compared to the entrance region. Therefore hadrontheraphy allows delivering higher doses in deep-seated tumours, killing malignant cells, and reducing the dose in healthy tissues [Kraft, 2000; Podgorsak, 2005].

For treatment planning in hadrontherapy it is essential to know accurately the beam penetration range in human tissue, which is usually represented by liquid water, since it is an excellent tissue-like phantom material for determination of absorbed dose [ICRU, 1998]. However, measurements in phantoms made of materials different from liquid water (even sometimes solid materials) can be performed in order to simplify the experimental set-up.

The ion beam penetration range in a material is often characterized by the water equivalent thickness (WET), which measures the thickness of liquid water needed to stop the ion beam in the same manner that a certain thickness of the given material. A proper evaluation of the water equivalent properties of materials has to take into account the main effects in the energy deposition of the beam. In this context, radiation transport codes are especially useful, since they can handle all these interactions to evaluate their effect in the depth-dose distribution and in the water-equivalent depth [Paganetti, 2009]. Therefore, for a precise comparison of the materials and liquid water measurements, the water equivalent thickness of the materials must be accurately determined, as well as the position and magnitude of their Bragg peak.

The aim of this work is to simulate the depth-dose profile of proton beams in a wide range of incident energies commonly used in hadrontheraphy (50 MeV to 200 MeV) and for several materials currently used in proton dosimetry, such as liquid water, polystyrene (PS), polymethyl methacrylate (PMMA), graphite, aluminum, titanium, copper and gold. We apply the SEICS code (Simulation of Energetic Ions and Clusters through Solids) based in a combination of Molecular Dynamic and Monte carlo

procedures to follow the trajectories of the incident projectiles [Garcia-Molina et al., 2011], by taking into account the electronic stopping power (including statistical fluctuations through the energy-loss straggling), multiple elastic scattering collisions, electronic charge-exchange processes and nuclear fragmentation reactions. An important feature of our simulation is the use of accurate values for the electronic energy-loss magnitudes, which are calculated within the dielectric formalism and the MELF-GOS model (Mermin Energy Loss Function- Generalized Oscillator Strength) [Abril et al., 1998; Heredia-Avalos et al., 2005], where the target excitation spectrum is modelled by a self-consistent condensed phase description of its energy-loss function, based on experimentally available optical data, over the entire energy and momentum transfers space.

The water equivalence thickness and other characteristic parameters of the Bragg curves of materials of significance in proton dosimetry are compared with the results obtained for liquid water from the simulated depth-dose distributions. There are several analytical calculations and simulations of the WET corresponding to different materials for energetic proton beams [ICRU, 1993; Palmans and Verhaegen, 1997; IAEA, 2000, Palmans et al., 2002; Zhang and Newhauser, 2009; Moyers et al., 2010; Zhang et al., 2010, Al-Sulaiti et al., 2010]. Some of these publications are based in the ratio of the continuous-slowing-down approximation (CSDA) ranges (in g/cm^2) in water and in the analyzed target [IAEA, 2000; Al-Sulaiti et al., 2010]. Other works use simple deterministic formulas, where the proton energy loss was derived from the Bragg-Kleeman rule or from the Bethe-Bloch equation without considering the change in the proton energy, obtaining WET values with accuracies around 1 mm [Zhang and Newhauser, 2009; Zhang et al., 2010]. Other authors use Monte Carlo codes, such as PTRAN [Palmans and Verhaegen, 1997; Palmans et al., 2002] or MCNPX [Al-Sulaiti et al., 2010], where the stopping powers are taken from the ICRU report 49 [ICRU 1993] by applying Bragg's rule for compound targets, and where the influence of the fragmentation nuclear interactions has been investigated. The SEICS simulation code incorporates an accurate treatment of the electronic stopping force and the energy-loss straggling (the main responsible of the Bragg peak position and its shape, respectively), which is determined taking into account a realistic description of the target electronic excitation spectrum in the condensed phase, based in the experimental optical energy loss function of the target [Abril et al., 1998; Heredia-Avalos et al., 2005].

This paper is structurated as follow. The main aspects of the SEICS simulation code are presented in section 2, whereas the depth dose distributions and the water equivalent characteristics obtained by this code are presented in section 3 for a broad range of incident proton energies and for several materials of interest in dosimetry measurements. Finally, the main conclusions of this work are summarized in section 4.

2.- Simulation procedure

The SEICS code (Simulation of Energetic Ions and Clusters through Solids) simulates the transport of energetic ions through condensed media. The detailed motion of the projectile is described by a Molecular Dynamics method, whereas a Monte Carlo procedure is employed to treat the statistical nature of the electronic and the elastic scattering, the electron charge-exchange processes between the projectile and the target and the nuclear fragmentation of the projectile due to non-elastic nuclear scattering processes [Garcia-Molina et al., 2011, Garcia-Molina et al., 2012a]. As a consequence of this treatment, the SEICS code provides the depth dose as well as the spatial profiles of energetic projectiles in condensed target.

Solving numerically the equation of motion of the projectiles, we follow their trajectory in the media until they have a cutoff energy of 250 eV. When the projectile has an instantaneous position $\vec{r}(t)$ and velocity $\vec{v}(t)$ and the force that act on it is $\vec{F}(t)$, the projectile new position and velocity after a time step Δt are given by:

$$\vec{r}(t+\Delta t) = \vec{r}(t) + \vec{v}(t)\Delta t + \frac{\vec{F}(t)}{2M}(\Delta t)^2\left[1-\left(v(t)/c\right)^2\right]^{3/2}, \quad (1)$$

$$\vec{v}(t+\Delta t) = \vec{v}(t) + \frac{\vec{F}(t)+\vec{F}(t\Delta t)}{2M}\Delta t\left[1-\left(v(t)/c\right)^2\right]^{3/2}, \quad (2)$$

where M is the mass of the projectile, c is the speed of light and the terms in brackets are an *ad hoc* modification of the original Verlet's algorithm to account for the relativistic velocity of the projectile. Note that for the typical projectile energies used in hadrontherapy (several hundred of MeV/u), it is necessary to take into account the relavitistic character of the projectile.

The force $\vec{F}(t)$ felt by the projectile, with a charge state q, is mainly due to inelastic interactions with the target electrons. However to take into account the stochastic nature

of these interactions, in the simulation code the electronic stopping force is randomly sampled according to a Gaussian distribution, where the mean value is the stopping power, S_q, and the standard desviation is related with the energy-loss straggling, Ω_q^2 [Garcia-Molina et al., 2012a].

The energy-loss magnitudes S_q and Ω_q^2, used as input in the SEICS code, are calculated by the dielectric formalism, which is based in the plane-wave Born approximation, and where the target description enters through its energy loss function (ELF), which is calculated by the MELF-GOS model [Abril et al., 1998, Heredia-Avalos et al., 2005]. Thus, the outer electron excitations are described by a sum of Mermin-type ELF [Mermin, 1970], which is fitted to the experimental optical data, whereas the inner-shell electrons are accounted for by their generalized oscillator strengths in the hydrogenic approach. This model incorporates the individual and collective excitations of the target as well as aggregation and chemical effects inherent to the condensed phase, since the target ELF has been fitted to available experimental optical data. Another advantage of the MELF-GOS model is that once the fit at the optical limit (i.e., momentum transfer $k = 0$) is made, the ELF is automatically extended to any momentum transfer ($k \neq 0$), and no extra dispersion relations are necessary [Garcia-Molina et al., 2012b].

The total stopping power is obtained by a weighted sum of the stopping powers for each different charge state q that the projectile can acquire during its travel through the target and the fractions of these charge states at the dynamical equilibrium. In figure 1 we show our calculated stopping power S for a proton beam as a function of its incident energy for several materials of interest in dosimetry, such as liquid water [Garcia-Molina et al., 2009], polystyrene (PS), PMMA [de Vera et al., 2011], graphite [Garcia-Molina et al., 2006], Al [Denton et al., 2008], Ti [Moreno-Marin et al., 2006], Cu [Abril et al., 1998] and Au [Denton et al., 2008]. As can be seen in the above references, a good agreement with experimental data was obtained; in particular, the stopping power of liquid water for proton beams has been widely discussed and compared with experimental data and other theoretical calculations [Garcia-Molina et al., 2012b].

In order to save computer time, at high proton energies ($E \geq 10$ MeV for protons) the SEICS code uses the analytical relativistic Bethe formula for the stopping power,

$$S = \frac{4\pi e^4 Z_2 Z_1^2 N}{v^2} \ln\left(\frac{2m_e v^2}{I(1-(v/c)^2)} - (v/c)^2 \right), \quad (3)$$

where Z_1 and Z_2 are, respectivately, the atomic number of the projectile and the target (electrons per molecule in the case of compounds), N is the atomic or molecular density of the target, m_e is the electron mass, v is the projectile velocity, and I is the mean excitation energy of the target, which only depends on its electronic structure [Fano, 1963]. In Table I the I values for all the materials treated in this work are presented, which are calculated using the MELF-GOS method [de Vera et al., 2011, Abril et al., 2012].

Table I.- Mean excitation energy I of several materials frequently used in hadrontherapy, obtained by the MELF-GOS model. The target chemical formula, atomic number Z_2 (or number of electrons per molecule for compounds) and density are also shown.

Target	**Chemical formula**	**Z_2**	**Density (g/cm^3)**	***I* (eV)**
Liquid water	H_2O	10	1	79.4
Polystyrene (PS)	$(C_8H_8)_n$	56	1.06	72.1
PMMA	$(C_5H_5O_2)_n$	51	1.188	70.3
Graphite		6	2.25	83.95
Al		13	2.7	156.7
Ti		22	4.5	223.9
Cu		29	8.96	373.4
Au		79	19.3	755.8

Simulations with the SEICS code indicate that electronic interactions is the major responsible of the energy loss of the projectile, so the stopping power determines mainly the position of the Bragg peak, whereas the energy-loss straggling is the major responsible of its shape [Garcia-Molina et al., 2011].

On the other hand, multiple elastic scattering are very frequent events that modify the trajectory of the projectile (providing its angular deflection) and contribute to the energy-loss at low energies, especially at the distal part of the Bragg peak, which affects the range of the projectile. The multiple elastic scattering of the projectile with the target nuclei is accounted for in the SEICS simulation through a Monte Carlo algorithm [Moller et al., 1975; Zajfman et al., 1990]. Moreover, electron capture and loss processes are also considered dynamically along the projectile travel.

Finally, nuclear fragmentation reactions between primary protons and target nuclei are included in the simulation, since they can affect the energy deposition process. Therefore, part of the total depth-dose distribution in proton therapy will be due to secondary protons, deuterons, tritons, ^{3}He and α-particles liberated in the inelastic nuclear interactions. In the simulation, the primary protons that undergo a fragmentation reaction are eliminated from the beam whereas the generated secondary charged particles will deposit their energy at the location of their production.

The primary protons are removed from the beam by a Monte Carlo algorithm according to their total nuclear reaction cross sections depending on their instantaneous energy, which are taking from the ICRU tables [ICRU, 2000]. For compound targets, fragmentation cross sections are calculated applying the Bragg's rule [Bragg and Kleeman, 1905] to the elemental atoms than constitute each target. Only a fraction of the energy of the secondary particles is deposited locally according to the ICRU tables for protons or for heavier particles [ICRU, 2000]. The contribution to the depth-dose distribution due to the secondary protons agrees rather well with the simulation presented by Medin and Andreo [Medin and Andreo, 1997] where the transport of these secondary protons are included, except near the target surface [de Vera et al., 2013]. In our approach, we assume that the energy transferred to neutrons or photons leaves the target without contributing to the dose distribution [Medin and Andreo, 1997]. However, a Monte Carlo study of secondary neutrons generated in proton therapy in several phantom materials has been reported in Ref. [Dowdell et al., 2007]. In order to verify the validation of our simulation, we have compared our results with experimental depth-

dose distribution of protons in liquid water for energies around 120 MeV to 220 MeV [Zhang et al., 2011] obtaining a good agreement [de Vera et al., 2013].

3.- Results and discussion

From the SEICS simulation code, the Bragg curves of proton beams with energies from 50 MeV to 200 MeV are obtained for materials with low (liquid water, polystyrene, PMMA), medium (graphite, Al), and high (Ti, Cu, Au) density, relevant in dosimetric studies. The depth-dose profiles of 100 MeV protons in these materials are shown in figure 2. The results for solid plastics such as polystyrene or PMMA present depth-dose characteristics comparable to those of liquid water, whereas the differences increase for graphite and aluminum. Materials with high density such as Ti, Cu and Au have also high stopping power for proton beams compared with liquid water, therefore the largest differences in the Bragg peak with respect to liquid water are observed for those materials. As it can be noted, the stopping power for each material determines the position of the Bragg peak, according to the features shown in figure 1. Despite the importance of using accurate values for the stopping power S in dosimetry, there is not a general consensus about the best values of S which have to be employed in each case.

In proton dosimetry the radiological thickness of a material is commonly expressed in terms of water-equivalent thickness (WET), which represents the thickness of water (in g/cm^2) that causes a proton beam to lose the same amount of energy as the beam would lose in the studied material [IAEA, 2000],

$$\mathrm{WET} = z_{\mathrm{water}}\rho_{\mathrm{water}} = z_{\mathrm{mat}}\rho_{\mathrm{mat}}\,C\,, \qquad (4)$$

where z_{water}, ρ_{water} and z_{mat}, ρ_{mat} are, respectively, the thickness (in cm) and density (in g/cm^3) of liquid water and the target material; C is the depth-scaling factor. Sometimes it is convenient to characterize the beam penetration range by the water equivalent ratio (WER), which is the ratio of WET to material thickness (in g/cm^2), i.e., WER is the ratio of water thickness (in cm) to material thickness (in cm),

$$\mathrm{WER} = \frac{z_{\mathrm{water}}}{z_{\mathrm{mat}}} = \frac{\rho_{\mathrm{mat}}}{\rho_{\mathrm{water}}} C \,. \tag{5}$$

The adimensional magnitude WER is easier to compare with results from measurements or calculations obtained at different conditions, and also their values are approximately constant as a function of the projectile energy [Palmans and Verhaegen, 1997].

A procedure proposed to calculate WER is through the ratio of the continuous-slowing-down approximation (CSDA) for proton ranges in water and in the material of interest [IAEA, 2000; Palmans et al., 2002]. Given the approximate nature of the CSDA, more accurate values of WER will be obtained using simulation codes where a realistic description of the different processes that occurs in the proton trajectories through the target are taken into account. Therefore, from the simulated depth-dose profiles, the range of the projectiles can be defined as the depth z_{80} where the distal part of the Bragg peak falls to 80% of the maximum dose [Palmans et al., 2002; Al-Suliati et al., 2010; Palmans et al., 2011]. Then WER will be calculated as:

$$\mathrm{WER} = \frac{z_{80,\mathrm{water}}}{z_{80,\mathrm{mat}}} \,. \tag{6}$$

From the simulation code SEICS, where the most relevant processes in the proton transport through the stopping medium are included, the depth dose distributions of protons in several materials are calculated and compared with those obtained for liquid water. Table II shows the water equivalent ratio (WER) of protons with energies from 50 MeV to 200 MeV. We analyzed solid plastics used frequenly as phantoms of liquid water or in modulator wheels, such as PMMA or polystyrene [Karger et al., 2010]. Also in graphite calorimeters the conversion from dose-to-graphite to dose-to-water and WER values are necessary for an accurate dosimetry [Palmans et al., 2004]. Finally the water equivalence of other materials often involved in proton dosimetry setups such as Al, Ti, Cu and Au are presented. In the simulation code the nuclear fragmentation processes are included for all the materials [de Vera et al., 2012], except for Ti and Au targets.

We find that, except for Au, the WER values are almost independent of the energy of the incident proton beams and also are insensible to non-elastic nuclear interactions. In Table II we also compare the WER with experimental measurements for PMMA and Al [Moyers et al., 2010] and with analytical calculations for PMMA, PS and Al [Zhang

and Newhauser, 2009; Zhang, et al., 2010] obtaining a good agreement. The WER results obtained from our simulation are consistent with the data from the IAEA report for PMMA (1.160) [IAEA, 2000], from Newhauser, 2001 (1.162), and with the data reported by Schneider et al., 2002 for 177 MeV proton beam in PMMA (1.14) and in Al (2.08) targets.

Table II.- Water equivalent ratio, WER, for various incident proton energies, calculated from the SEICS code, for the materials discussed in this work. A comparison with experimental data from Moyers et al., 2010 and calculated values from Zhang and Newhauser, 2009 and from Zhang, et al., 2010 (shown in parenthesis) is also presented.

Target / E (MeV)	PS	PMMA	PMMA Moyers et al., 2010	PMMA Zhang and Newhauser, 2009 (Zhang et al., 2010)	Graphite	Al	Al Moyers, et al., 2010	Al Zhang and Newhauser, 2009 (Zhang et al., 2010)	Ti	Cu	Au
50	1.043	1.177			2.009	2.101		2.069	5.623	3.136	9.104
75	1.042	1.175			2.009	2.114			5.722	3.168	9.395
100	1.042	1.174		1.158	2.010	2.123		2.095-2.091	5.786	3.189	9.576
125	1.041	1.173			2.010	2.131			5.844	3.208	9.741
135		1.173	1.170	(1.158)		2.131	2.130	(2.097)			
150	1.040	1.173		1.158	2.010	2.133	2.114	2.106-2.104	5.863	3.214	9.792
175	1.040	1.173	1.162	(1.158)	2.010	2.137	2.114	(2.107)	5.889	3.225	9.868
200	1.040	1.172		1.157	2.010	2.139		2.113-2.112	5.900	3.229	9.900
225		1.172	1.167	(1.158)		2.144	2.145	(2.116)			

On the other hand, besides the WER values, the Bragg peak can be characterized by other parameters such as the depth z_{max} corresponding to the maximum dose Φ_{max}, the depth z_{50} at the distal part of the Bragg peak where the dose falls to 50% of its maximum value, and the distance Δz_{50} which corresponds to the width of the Bragg peak when the dose is at 50% of its maximum value. In figure 3 all these parameters are represented in relation to their values in liquid water, as a function of the proton energy and for the targets discussed in this work. In general, all these parameters are almost independent of the energy of the proton beam, except the ratio $\Phi_{max} / \Phi_{max-water}$ for gold, where an increase with the energy is observed. Also, the values of the parameters $z_{max} / z_{max\text{-}water}$ and $z_{50} / z_{50\text{-}water}$ are similar for all the energies and materials, and they are insensible to the nuclear fragmentation processes. However, although the parameter Φ_{max} decreases when nuclear fragmentation is included in the simulation, the ratio $\Phi_{max} / \Phi_{max-water}$ is independent of the nuclear fragmentation reactions. Also the width Δz_{50} increases when nuclear fragmentation interactions are included in the simulation, however the ratio $\Delta z_{50} / \Delta z_{50\text{-}water}$ remains constant. From the values of the characteristic parameters of the depth-dose profile depicted in fig. 3 and shown in Table II relative to liquid water, we conclude that polystyrene and PMMA are the materials having all the parameters analyzed here closer to unity. As a consequence, the Bragg curves for those materials with densities and stopping powers similar to those corresponding to liquid water can operate as adequate phantom of liquid water since they present the best water equivalent properties of all the materials analyzed in this work. Also, our results indicate that the larger the stopping power of the protons in a material in comparation with liquid water the bigger differences appear in the characteristic depth-dose parameters. So, materials with large density and large stopping power will provide the largest perturbations when used in proton dosimetry.

4.- Summary

The Bragg curves of proton beams, with energies from 50 to 200 MeV, in several materials of interest in dosimetry (such as liquid water, PS, PMMA, graphite, Al, Ti, Cu and Au), have been simulated by the SEICS code. The simulation includes the significant processes that take place between the projectile and the target, such as electronic energy-loss (including stochastic fluctuations through the energy-loss straggling), multiple elastic scattering, charge-exchange processes and nuclear fragmentation reactions. A comparison of several parameters characterizing the simulated depth-dose profiles of the materials with those corresponding to liquid water, including the water-equivalence ratio, shows that they do not depend of the proton energy or the nuclear fragmentation. We conclude that materials having stopping power similar to liquid water (in the range of proton energies considered in this work), such as PS and PMMA, present almost all their parameters relevant in dosimetry analogous to liquid water, being therefore well suited for use as phantom of liquid water in dosimetric measurements.

Acknowledgements

This work has been financially supported by the Spanish Ministerio de Ciencia e Innovación, Project FIS2010-17225. PdV thanks the Conselleria d'Educació, Formació i Ocupació de la Generalitat Valenciana for its support under the VALi+d program. This research has been developed as part of the COST Action MP 1002, Nanoscale Insights into Ion Beam Cancer Therapy.

References

Abril, I., Garcia-Molina, R., Denton, C. D., Pérez-Pérez, F. J., Arista, N. R., 1998. Dielectric description of wakes and stopping powers in solids. Phys. Rev. A 58, 357-366.

Abril, I., Garcia-Molina, de Vera, P., Kyriakou, I., Emfietzoglou, D., 2012. Inelastic collisions of energetic protons in biological media, in "Theory of heavy particle collisions with prospects for applications to hadron therapy", Adv. Quant. Chem. (edited by Dz. Belkic), in print (2013).

Al-Sulaiti, L., Shipley, D., Thomas, R., Kacperek, A., Regan, P., Palmans, H., 2010. Water equivalence of various materials for clinical proton dosimetry by experiment and Monte Carlo simulation. Nucl. Instrum. Meth. Phys. Res. A 619, 344–347.

Bragg, W. H., Kleeman, R., 1905. On the alpha particles of radium and their loss of range in passing through various atoms and molecules. Philos. Mag. 10, 318–340.

Denton, C. D., Abril, I., Garcia-Molina, R., Moreno-Marín, J. C., Heredia-Avalos, S., 2008. Influence of the description of the target energy-loss function on the energy loss of swift proyectiles. Surf. Inter. Anal. 40, 1481–1487.

de Vera, P., Abril, I., Garcia-Molina, R., 2011. Inelastic scattering of electron and light ion beams in organic polymers. J. Appl. Phys. 109, 094901-1 –8.

de Vera, P. , Abril, I., Garcia-Molina, R., 2013. In preparation.

Dowdell, S., Clasie, B., Wroe, A., Guatelli, S., Metcalfe, P., Schulte, R., Rosenfeld, A., 2009. Tissue equivalency of phantom materials for neutron dosimetry in proton therapy. Med. Phys. 36, 5412- 5419.

Fano, U., 1963. Penetration of protons, alpha particles, and mesons, Annu. Rev. Nucl. Sci. 13, 1.

Garcia-Molina, R., Abril, I., Denton, C. D., Heredia-Avalos, S., 2006. Allotropic effects on the energy loss of swift H^+ and He^+ ion beams through thin foils. Nucl. Instrum. Meth. Phys. Res. B 249, 6–12.

Garcia-Molina, R., Abril, I., Denton, C. D., Heredia-Avalos, S., Kyriakou, I., Emfietzoglou, D., 2009. Calculated depth-dose distributions for H^+ and He^+ beams in liquid water. Nucl. Instrum. Meth. B 267, 2647-2652.

Garcia-Molina, R., Abril, I., Heredia-Avalos, S., Kyriakou, I., Emfietzoglou, D., 2011. A combined Molecular Dynamics and Monte Carlo simulation of the spatial distribution of energy deposition by proton beams in liquid water. Phys. Med. Biol. 56, 6475-6493.

Garcia-Molina, R., Abril, I., de Vera, P., Kyriakou, I., Emfietzoglou, D., 2012a. Proton beam irradiation of liquid water: A combined Molecular Dynamics and Monte Carlo simulation study of the Bragg peak profile, Ch. 8 pp. 271-304 in Fast Ion-Atom and Ion-Molecule Collisions, ed. D. Belkic, World Scientic.

Garcia-Molina, R., Abril, I., Kyriakou, I., Emfietzoglou, D., 2012b. Energy loss of swift protons in liquid water: Role of optical data input and extension algorithms, Ch. 15 pp. 239-262 in Radiation Damage in Biomolecular Systems, eds. G. García Gómez-Tejedor, M.C. Fuss, Springer, Dordrecht.

Heredia-Avalos, S., Garcia-Molina, R., Fernández-Varea, J. M., Abril, I., 2005. Calculated energy loss of swift He, Li, B, and N ions in SiO_2, Al_2O_3, and ZrO_2. Phys. Rev. A 72, 052902-1-9.

ICRU, 1993. Stopping Powers and Ranges for Protons and Alpha Particles. International Commission on Radiation Units and Measurements. Report 49, Bethesda, MD.

ICRU, 1998. Clinical Proton Dosimetry. Part I: Beam Production, Beam Delivery and Measurement of Absorbed Dose. International Commission on Radiation Units and Measurements. Report 59. Bethesda, MD.

ICRU, 2000. Nuclear data for neutron and proton radiotherapy and for radiation protection, International Commission on Radiation Units and Measurements. Report 63, Bethesda.

IAEA, 2000. Absorbed dose determination in external beam radiotherapy: An internal code of practice for dosimetry based on standards of absorbed dose to water. International Atomic Energy Agency, Vienna.

Karger, C. P., Jäkel, O., Palmans H., Kanai, T., 2010. Dosimetry for ion beam radiotherapy. Phys. Med. Biol. 55, R193–R234.

Kraft, G., 2000. Tumor Therapy with Heavy Charged Particles. Prog. Part. Nucl. Phys. 45, S473–544.

Medin, J., Andreo, P., 1997. Monte Carlo calculated stopping-power ratios, water/air, for clinical proton dosimetry (50–250 MeV). Phys. Med. Biol. 42, 89–105.

Mermin, N. D., 1970. Lindhard dielectric function in the relaxation-time approximation. Phys. Rev. B 1, 2362-2363.

Möller W., Pospiech G., Schrieder G., 1975. Multiple scattering calculations on ions passing through thin amorphous foils. Nucl. Instrum. Methods 130, 265–270.

Moreno-Marín, J. C., Abril, I., Heredia-Avalos, S., Garcia-Molina, R., 2006. Electronic energy loss of swift H^+ and He^+ ions in solids with material science applications. Nucl. Instrum. Meth. Phys. Res. B 249, 29–33.

Moyers, M. F., Sardesai, M., Sun, S., Miller, D. W., 2010. Ion stopping powers and CT numbers. Med. Dosim. 35, 179-194.

Newhauser, W., 2001. Dosimetry for the gantry beams at the northeast proton therapy center: Part I. Dimensions and geometric relationships. Massachusetts General Hospital Report HD-112. Boston.

Paganetti, H., 2009. Dose to water versus dose to medium in proton beam therapy. Phys. Med. Biol. 54, 4399–4421.

Palmans, H., Verhaegen, F., 1997. Calculated depth dose distributions for proton beams in some low-*Z* materials. Phys. Med. Biol. 42, 1175–1183.

Palmans, H., Symons, J. E., Denis, J.-M., de Kock, E. A., Jones, D. T. L., Vynckier, S., 2002. Fluence correction factors in plastic phantoms for clinical proton beams. Phys. Med. Biol. 47, 3055-3071.

Palmans, H., Thomas, R., Simon, M., Duane, S., Kacperek, A., Du Sautoy, A., Verhaegen, F., 2004. A small-body portable graphite calorimeter for dosimetry in low-energy clinical proton beams. Phys. Med. Biol. 49, 3737-3749.

Palmans, H., Al-Sulaiti, L., Andreo, P., Thomas, R. A. S., Shipley, D. R. S., Martinkovi, J., Kacperek, A., 2011. Conversion of dose-to-graphite to dose-to-water in a clinical proton beam, in Standards, Applications and Quality Assurance in Medical Radiation Dosimetry (DOS), IAEA Internacional Atomic Energy Agency, Vol.1, pags. 343-355, Viena.

Podgorsak, E. B., 2005. Radiation oncology physics: A handbook for teachers and students. International Atomic Energy Agency. Vienna.

Schneider, U., Pemler, P., Besserer, J., Dellert, M., Moosburger, M., de Boer, J., Pedroni, E., Boehringer, T., 2002. The water equivalence of solid materials used for dosimetry with small proton beams. Med. Phys. 29, 2946-2951.

Zajfman D., Both G., Kanter E. P., Vager Z., 1990. Multiple scattering of MeV atomic and molecular ions traversing ultrathin films. Phys. Rev. A 41, 2482–2488.

Zhang, R., Newhauser, W. D., 2009. Calculation of water equivalent thickness of materials of arbitrary density, elemental composition and thickness in proton beam irradiation. Phys. Med. Biol. 54, 1383–1395.

Zhang, R., Taddei, P. J., Fitzek, M. M., Newhauser, W. D., 2010. Water equivalent thickness values of materials used in beams of protons, helium, carbon and iron ions. Phys. Med. Biol. 55, 2481-2493.

Zhang, X., Liu, W., Li, Y., Li, X., Quan, M., Mohan, R., Anand, A., Sahoo, N., Gillin, M., Zhu, X. R., 2011. Parameterization of multiple Bragg curves for scanning proton beams using simultaneous fitting of multiple curves. Phys. Med. Biol. 56, 7725–7735.

Highlights

- Depth-dose profile of proton beams in dosimetric materials is simulated by the SEICS code.
- The targets studied are liquid water, PMMA, polystyrene (PS), graphite, Al, Cu, Ti and Au.

- The water equivalent ratio is obtained from the simulated depth-dose distributions.
- PS and PMMA present depth-dose characteristics analogous to liquid water.
- PS and PMMA are well suited for use as phantom of liquid water in dosimetric measurements.

Figure Captions

Fig. 1.- Stopping power of several materials (liquid water, polystyrene (PS), PMMA, graphite, Al, Ti, Cu and Au) with interest in dosimetry, for an incident proton beam as a function of its energy, calculated with the dielectric formalism and the MELF-GOS model.

Fig. 2.- Depth dose distribution for a 100 MeV proton beam in different materials, as a function of the depth, obtained with the SEICS code.

Fig. 3.- Parameters that characterize the Bragg peak, such as z_{max}, Φ_{max}, z_{50} and Δz_{50}, relative to their values in liquid water, plotted as a function of the proton incident energies for the materials treated in this work. The results have been obtained with the SEICS code.

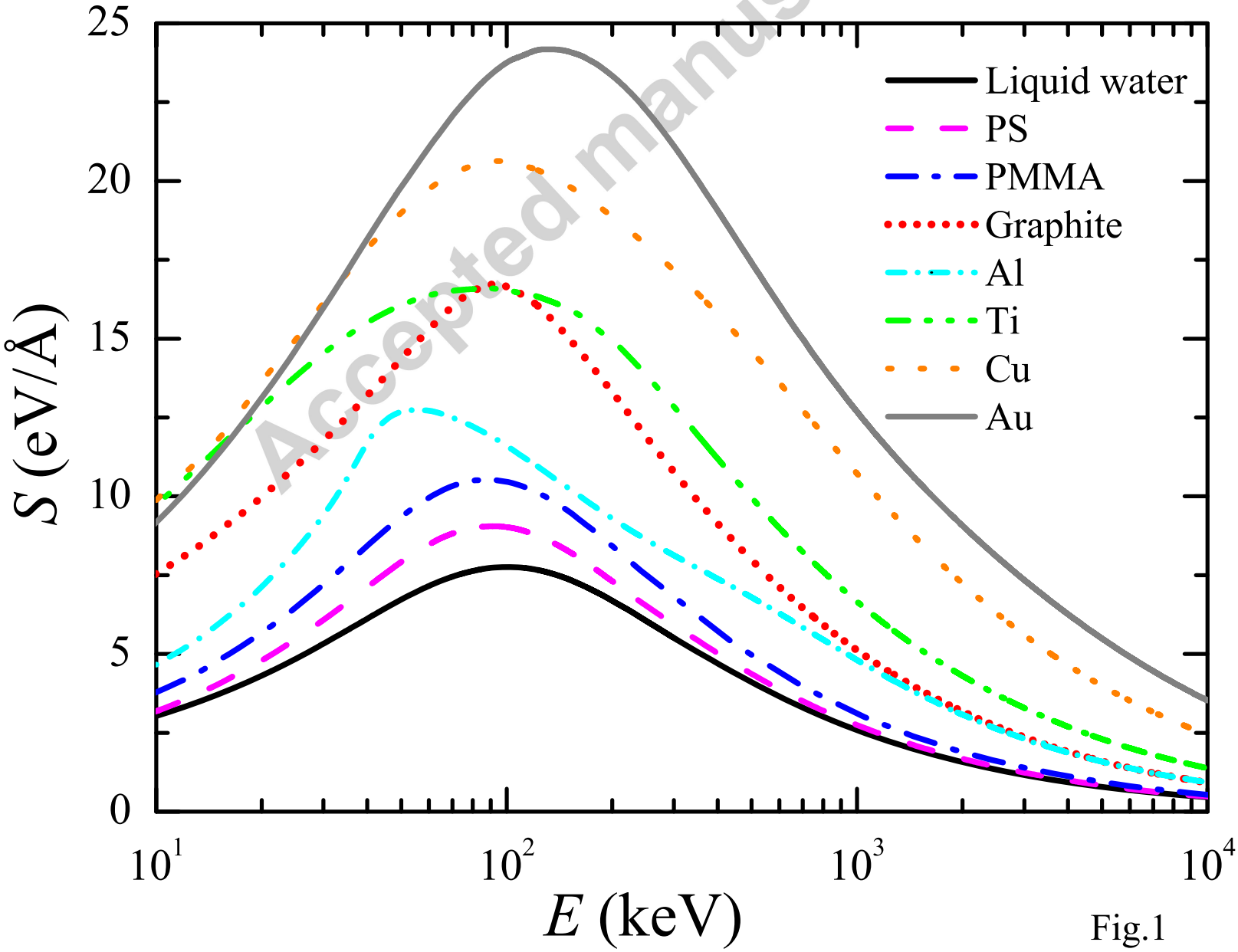

Fig.1

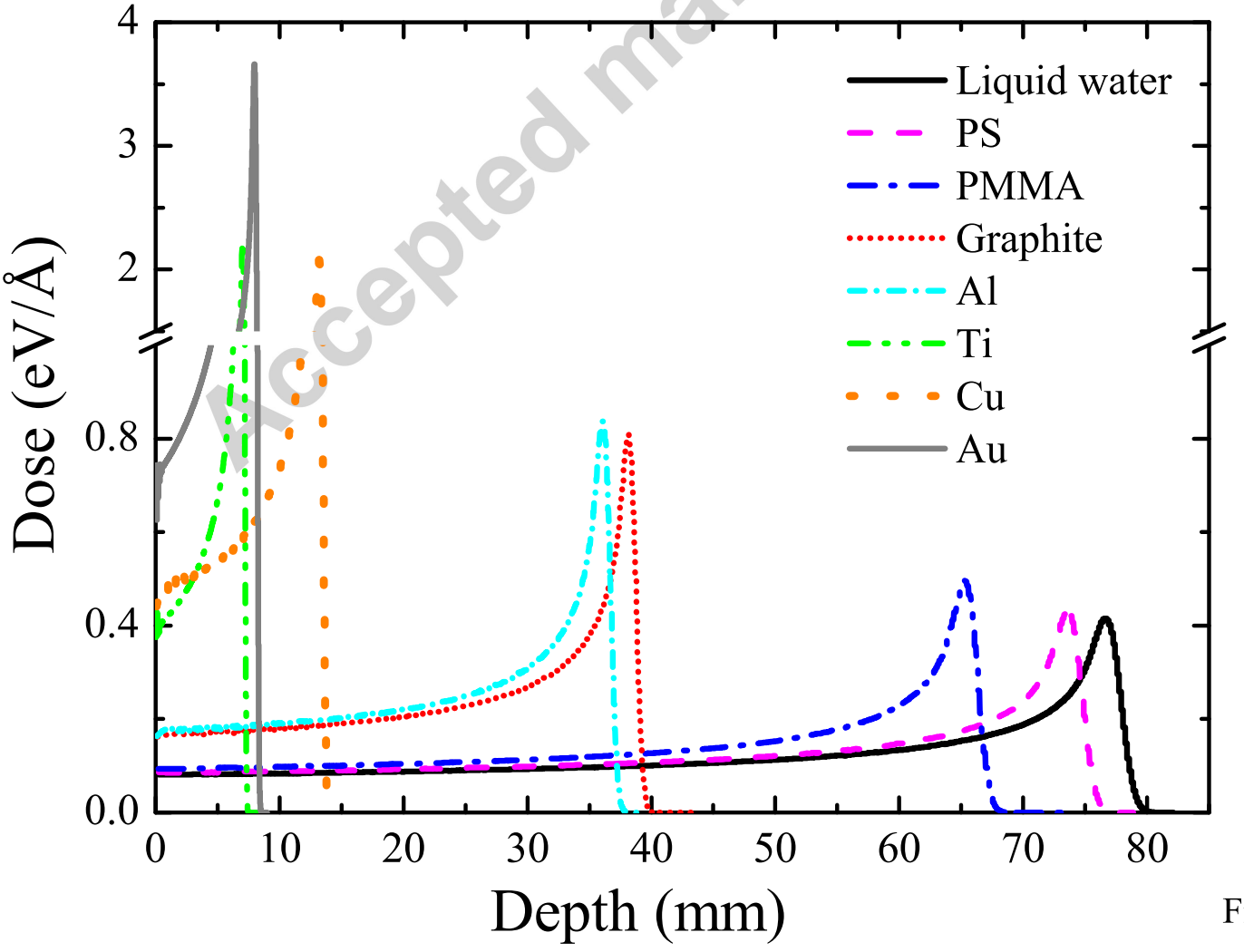

Fig.2

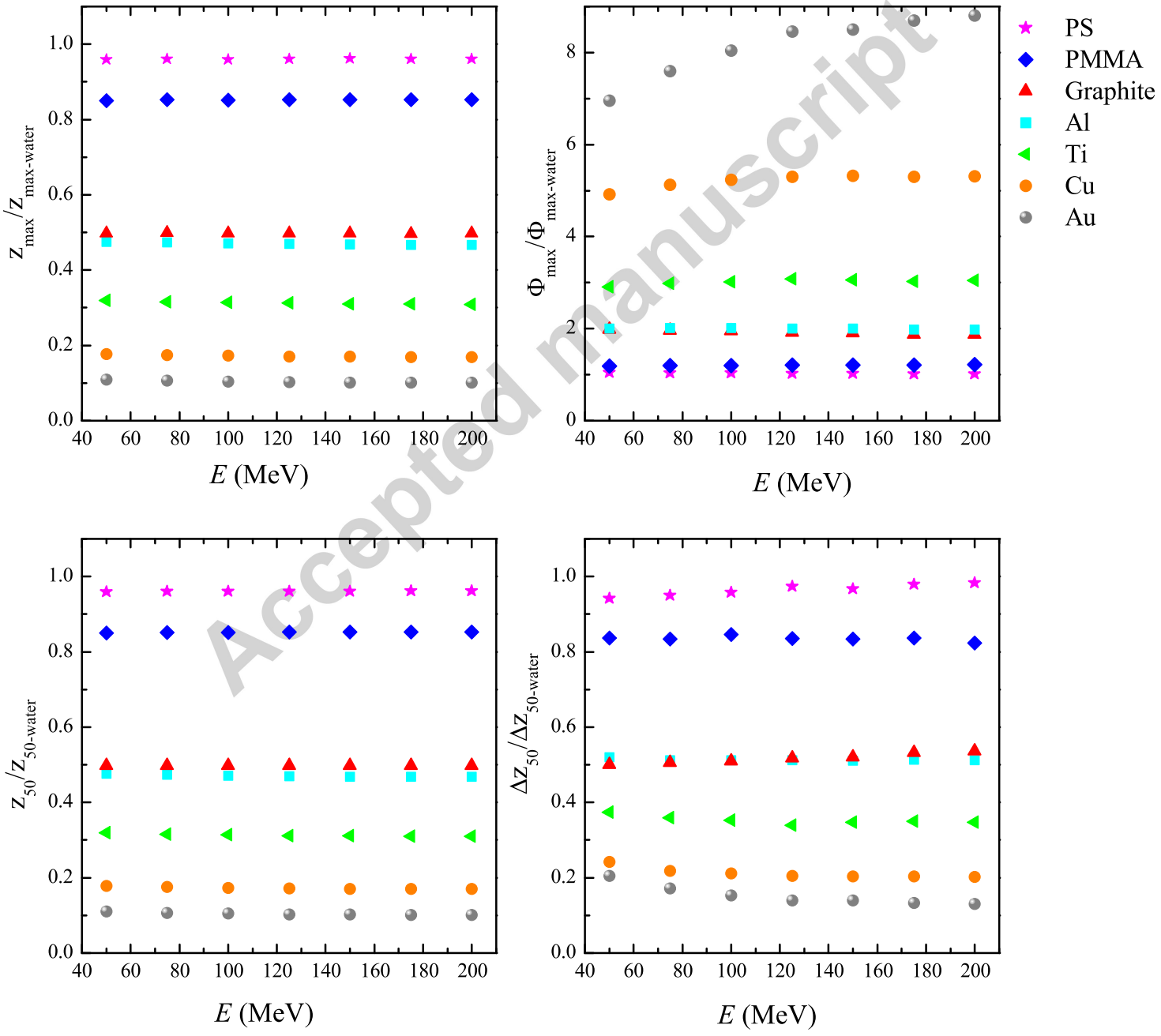

Fig.3